Journal of Alloys and Compounds 822 (2020) 153610

Contents lists available at ScienceDirect

Journal of Alloys and Compounds

journal homepage: http://www.elsevier.com/locate/jalcom

A combined experiment and first-principles study on lattice dynamics of thermoelectric $CuInTe_2$

Hao Yu [a, b, c], Ge Huang [c], Qing Peng [d], Zu-Cheng Chen [c], Hong-Jie Pang [c], Xiao-Ying Qin [a], Peng-Fei Qiu [e], Xun Shi [e], Li-Dong Chen [e], Xiao-Jia Chen [c, a, *]

[a] Key Laboratory of Materials Physics, Institute of Solid State Physics, Chinese Academy of Sciences, Hefei, 230031, China
[b] University of Science and Technology of China, Hefei, 23002645, China
[c] Center for High Pressure Science and Technology Advanced Research, Shanghai, 201203, China
[d] Physics Department, King Fahd University of Petroleum & Minerals, Dhahran 31261, Saudi Arabia
[e] State Key Laboratory of High Performance Ceramics and Superfine Microstructure, Shanghai Institute of Ceramics, Chinese Academy of Sciences, Shanghai, 200050, China

ARTICLE INFO

Article history:
Received 23 September 2019
Received in revised form
5 December 2019
Accepted 30 December 2019
Available online 7 January 2020

Keywords:
Chalcopyrite compounds
X-ray diffraction
Raman spectra
Ab initio calculations

ABSTRACT

Chalcopyrite compounds are promising high efficient thermoelectric materials. However, the relatively high lattice thermal conductivity at modest temperatures limits their performance. Here, we investigate the lattice dynamics in a polycrystalline $CuInTe_2$ with a combined experimental and computational approach. The phonon dispersion and density of states are computed using the density functional theory. Raman scattering is performed to investigate the phonon dynamical properties. Together with the bulk modulus from X-ray diffraction, the mode-Grüneisen parameters are determined. The low energy B_1^1 and E^2 modes characterize the weak anharmonicity, thus responsible for the high lattice thermal conductivity. Meanwhile, B_1^1 and E^2 modes display energy redshift under pressure. The softening and enhanced anharmonicity of these modes naturally result in the reduction of the thermal conductivity. Our study suggests that pressure is a routine to reduce the phonon heat conduction at modest temperatures in chalcopyrites.

1. Introduction

Due to the increasing demands of waste heat harvesting, thermoelectric (TE) materials and devices have drawn significant attention [1]. The performance of a TE material is scaled by the dimensionless figure of merit, namely zT [2,3]. Highly efficient TE materials should be characterized with large Seebeck coefficient S, high electrical conductivity σ, and low thermal conductivity κ [4,5]. The I-III-VI_2 ternary chalcopyrite compounds (I = Cu, Ag; III = Al, Ga, In; and VI = S, Se, Te) share a low symmetrical diamond-like structure. They have been previously applied in photovoltaic conversion and luminescent devices because of their moderate electrical conductivity and turnable band gaps [6–10]. Recently, the chalcopyrite compounds are studied as potential TE materials due to their universal low thermal conductivity at high temperatures and multi-band structure [11,12]. Among them, $CuInTe_2$ attracted much attention with the reported relative high zT value. For example, a maximum zT ~ 1.18 around 850 K has been reported benefiting from the large power factor (~ 13 $\mu Wcm^{-1}K^{-2}$) and low κ (~ 1 $Wm^{-1}K^{-1}$) [13,14]. The TE performance of a thermoelectric material can be dramatically enhanced under pressure [15–17]. The large zT enhancement of $CuInTe_2$ was mostly attributed to the reduction of κ by applying pressure. The diamond-like structure is of great interest for exhibiting dramatic potential TE properties [11,12,18]. However, the thermal conductivity at modest temperatures is relatively high. Similar situation is also observed in other chalcopyrite compounds, which definitely limits the average zT. Therefore, there is an urgent desire to tune the thermal conductivity at modest temperatures, which, however, is nontrivial.

For semiconductors, the thermal conductivity is mainly determined by lattice vibrations, namely, phonons. Therefore, the phonon information, including the phonon dispersion and anharmonic effects, are essential to understand the heat transport and to design low κ thermoelectric materials. Phonons with different energies usually characterize different velocities and scattering ratios,

* Corresponding author. Key Laboratory of Materials Physics, Institute of Solid State Physics, Chinese Academy of Sciences, Hefei, 230031, China.
E-mail address: xjchen@hpstar.ac.cn (X.-J. Chen).

https://doi.org/10.1016/j.jallcom.2019.153610
0925-8388/

thus occupying different proportions of κ [19,20]. Usually the acoustic branches were excessively emphasized in heat conduction due to the large velocities, while the thermal conductivity of optic branches was often ignored. Recently, the significance of the optic branches are reassessed. PbSe and PbTe, as examples, harvest about 25% and 22% of the thermal conductivity from the optic branches [21]. Moreover, the optic phonons, especially the branches with low energy, provide scattering channels for the acoustic branches [22]. Investigation the anharmonicity of the optic branches is beneficial to estimate the phonon scattering ratios. The phonon dispersion, density of states, and the anharmonic interplay among the phonon branches are essential to reveal the heat conduction. The phonon dispersion and density of states from theoretical calculation have been satisfactorily predicted conforming to the results from other techniques [23–25]. Meanwhile, the mode-Grüneisen parameters have been applied to estimate the phonon anharmonicity. However, experimental efforts to determine the mode-Grüneisen parameters still rare.

In this work, a *p*-type $CuInTe_2$ sample is chosen as an example to represent the phonon dynamic properties of the chalcopyrite compounds. The phonon dispersion and phonon density of state are calculated with density functional theory (DFT). The Raman scattering measurements under pressure are performed to study the optical phonons of $CuInTe_2$. The measurements of X-ray diffraction are carried out to obtain the equation of state and the bulk modulus. The Grüneisen parameter for each phonon mode is thus obtained by combining Raman scattering and X-ray diffraction results. Following this concept, we are able to show the detailed information of each phonon mode to understand the thermal transport properties. This may provide directions to reduce the thermal conductivity of the compounds with diamond-like structure.

2. Experiments

The high-quality *p*-type $CuInTe_2$ was prepared by melting the high purity elemental materials, namely, Cu, In and Te (99.999% in purity). The detailed synthetic procedure can be referred from the reference [14]. The pressure dependent Raman spectra were detected in a diamond anvil cell (DAC) with a cutlet size of 300 μm. Liquid Ne was chosen as the pressure medium to get reliable results. To obtain strong Raman spectrum signal, laser with 532 nm wavelength was chosen due to a relative large scattering cross section. Laser transports through a circular pinhole and is vertically focused on the flat surface of sample by a convex lens. The beam width was reduced to 0.12 mm by the pinhole, then compressed to 5∼8 μm by the convex lens. The laser power was kept at a low value of 1.5 mW to avoid heating effect. The laser power was determined by the laser powermeter (Thorlabs PM100D). The pressure dependent lattice evolution of $CuInTe_2$ was detected by using the synchrotron X-ray diffraction with the wavelength of 0.2910 Å. The spectra were collected in the PETRA III beamline P02.2 at DESY (Hamburg), a member of the Helmholtz Association. The grounded sample was pressed into densified bulk to get high resolution spectra. The DAC was prepared in the same way as that in Raman measurements. The Fit2D software was used to transform the raw XRD patterns into 2θ function. The GSAS software was applied to analyze the structure and lattice parameters based on the Rietveld refinement [26].

3. Ab Initio calculations

ab initio calculations are performed for the total energy, force, stress, geometry, and all other related properties within the frame of density functional theory. $CuInTe_2$ is a non-magnetic semiconductor. The crystal is tetragonal, with space group of $I\bar{4}2d$ and space group number of 122. The primitive unit cell contains 8 atoms in total, with two copper atoms, two indium atoms, and 4 tellurium atoms. The electrons explicitly included in the calculations are the $3s^2 3p6 3d^{10} 4s^1$ electrons (17 valence electrons) for Copper atoms, the $4d^{10} 5s^2 5p^1$ electrons (13 valence electrons) for Indium atoms, and the $5s^2 5p^4$ electrons (6 valence electrons) for Tellurium atoms. The high symmetry branches are selected according to the space group and crystal symmetry [27]. There are 12 high symmetry points, as Γ (0.0, 0.0, 0.0), N (0.0, 0.5, 0.0), P (0.25, 0.25, 0.25), Σ (-0.31228, 0.31228, 0.31228), Σ_1 (0.31228, −0.31228, −0.31228), X (0.0 0.0 0.5), Y (−0.12456, 0.12456, 0.5), Y_1 (0.5 0.5−0.12456), and Z (0.5 0.5−0.5). The k-point path is selected as $\Gamma->X->Y->\Sigma->\Gamma->Z->\Sigma_1->N->P->Y_1->Z|X->P$. The atomic vibrations are computed using CASTEP [28] at PBEsol level with norm conserving pseudopotentials. The inelastic scattering of monochromatic light with collective vibrations of crystals results in the energy of incident photons being shifted depending on spatial derivatives of the macroscopic polarization [29]. The calculation of the polarization for each branch displacement is achieved by a linear response formalism [30]. The energy cutoff for the plane-wave basis is 400 eV. The irreducible Brillouin Zone was sampled with a Gamma-centered $4 \times 4 \times 4$ *k*-mesh. The convergence of the total energy and forces is 1.0×10^{-5} eV and 1.0×10^{-2} eV/Å, respectively.

4. Results and discussion

ab initio calculations are performed to obtain the phonon dispersion and density of sates. The results of the phonon band structure and its corresponding density of states are shown in Fig. 1. The $CuInTe_2$ primitive cell contains 8 atoms, leading to 3 acoustic and 21 optic modes. The dynamics instability of a crystal structure is marked by the imaginary frequencies of phonon modes. A crystal is dynamically stable if its potential energy always increases against any combinations of atomic displacements. In the harmonic approximation, this is equivalent to the condition that all phonons have real and positive frequencies. Therefore, a imaginary frequency indicates dynamical instability of a system. In other words, the corrective atomic displacements could reduce the potential energy in the vicinity of the equilibrium atomic positions. As can be seen, no imaginary frequencies are presented among all phonon modes, which indicates that the crystal is dynamically stable. That all phonon modes are positive confirms that the atomic structures are in an energy-minimum position in a configurational space. The non-imaginary phonon band structure is a direct evidence that the crystal is stable in finite temperatures, agreeing well with experiments.

The optical phonon branches of $CuInTe_2$ at Γ point are represented as [31]: $3A_1+1A_2+3B_1+2B_2+12E$. Except B_2 modes, the rest modes are all Raman active. Due to the relative weak bonding forces, all the phonon bands are limited below 185 cm^{-1}. The phonons concentrate around 60, 120, and 180 cm^{-1}, mainly corresponding to the optic branches. Both the phonon dispersion and DOS curves show that there are non phonon energy bandgaps or forbidden energies in the whole range.

As a collective excitation, phonon determines many physical properties of a solid, including thermal, mechanical, and electrical properties. The phonon dispersion curves are very useful in prediction of the dynamical behaviors and the thermal conductivity. The group velocities are directly concerned with the slopes of the dispersion curves. The large slopes of the acoustic and low energy optic bands (below 160 cm^{-1}) suggest the large velocities. The low energy optic phonons, characterizing the high DOS and large velocities, play an important role in the heat conduction of $CuInTe_2$.

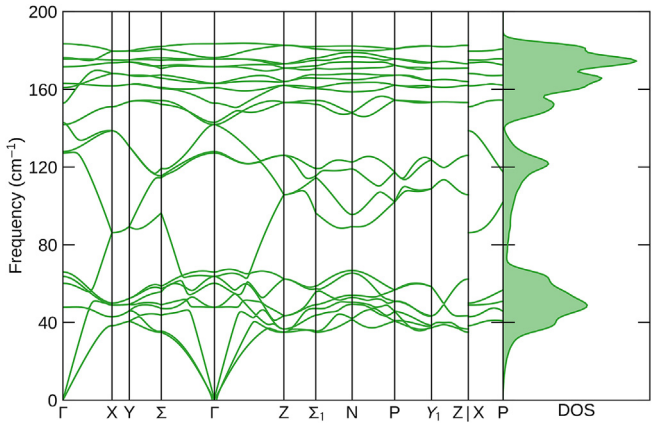

Fig. 1. The phonon dispersion and phonon density of states in $CuInTe_2$ from DFT calculations at 0 K.

The essential phonon scattering processes also have close relationship with the phonon dispersion. The continuous phonon band structure permits abundant scattering paths for all the phonon branches. Particularly, it is extremely important for the acoustic and low energy optic branches. Five optic phonon branches are suppressed below 65 cm^{-1} due to the weak bonding forces. These branches overlap with the acoustic branches, thus providing extra scattering paths among them. The anharmonic interactions of these bands will naturally be in favor of reducing their heat conduction.

The experiment of Raman scattering at 10 K has been carried out to verify the phonon dispersion and DOS obtained from *ab initio* computations. The spectrum is presented in the lower panel of Fig. 2. There are eight characteristic phonon bands at this temperature. These phonon bands roughly concentrate around 60, 130, and 180 cm^{-1}, corresponding to the calculated DOS. The calculated and experimental frequencies are collected in Table 1. These results match with each other, suggesting that the calculations are reliable. Then, the symmetry assignments of the experimental bands are determined as E^2, B^1_1, A^1_1, A_2, E^3, A^2_1, B^2_1, and A^3_1, respectively. Nine specific vibrations of the Raman active modes are presented in the upper panel of Fig. 2. As can be referred from the figure, the A_2, E^3, and A^21 modes are purely determined by the vibrations of Te or In atoms, while the rest phonon bands are all concerned with the vibrations of Cu, In, and Te atoms. Therefore, the defects on Cu, In, and Te sites are all effective phonon scattering centers. In the doped samples, such as $Cu_{1-x-\delta}Ag_xInTe_2$, $CuIn_{1-x}ZnTe_2$, and $CuIn_{1-x}GaTe_2$, κ values are significantly reduced from about 6 W/mK to 1.5 W/mK around 300 K [13,14,32,33]. As the chemical bonds Cu-Te and In-Te are different in the bonding angles and forces, the Cu^+ and In^{3+} atoms occupy the sites of distorted Cu-Te-In tetrahedrons. Based on this image, the vibrational modes can be treated as the deformations of Cu-In-Te tetrahedrons and also the relative vibrations between them. The asymmetric bonds lead to the low energy optic bands and the anharmonic potential field, thus determining the phonon dynamic behaviors.

For thermoelectric applications, the phonon dynamical behaviors are usually focused to quantify the heat conduction of semiconductors. In this given $CuInTe_2$ structure, the thermal transport properties are mainly determined by the anharmonic effect in the interested temperature range, which is directly concerned with the Grüneisen parameters γ. As can be referred from the theoretical calculations, the phonon dynamical behaviors of $CuInTe_2$ are highly frequency dependent. It's necessary to determine the mode-Grüneisen parameters of the various phonon branches. Grüneisen parameter is defined as: $\gamma_i = -d\ln\omega_i/d\ln V$, where ω_i is the frequency

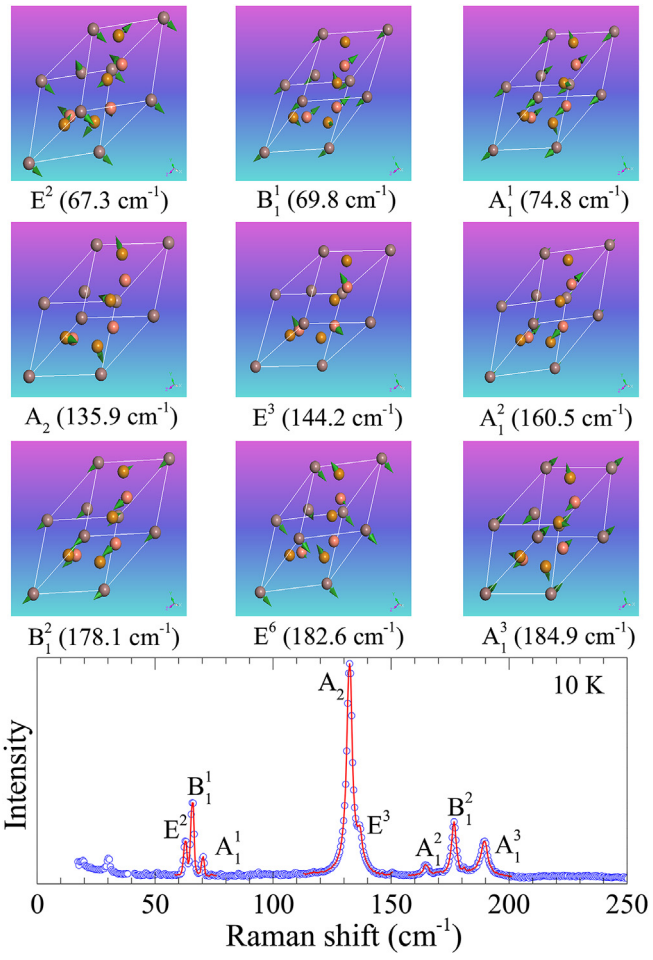

Fig. 2. The atomic vibrations of Raman active modes predicted by *abinitio* calculations. The phonon symmetry assignment and frequencies (at 0 K) are shown below these configurations. The lower panel presents the Raman spectra collected at 10 K.

Table 1
Comparison of the calculated Raman frequencies ω_{cal} (cm^{-1}) with the experimental results ω_{10K} (cm^{-1}).

A	ω_{Cal}	74.8	135.9	160.5	184.9		
	ω_{10K}	70.4±0.5	132.4±0.4	164.2±0.4	187.8±0.4		
B	ω_{Cal}	69.8	178.1	182.8			
	ω_{10K}	66.1±0.5	176.7±0.4	–			
E	ω_{Cal}	51.4	67.3	144.2	171.4	180.8	182.6
	ω_{10K}	–	62.7±0.4	137.1±0.6	–	–	–

of a phonon mode, and V is the volume of the crystal. Similar with the thermal expansion, the frequency shift induced by lattice compression is also attributed to the phonon anharmonicity [34–37]. Then, we get the γ_i expression as:

$$\gamma_i = -\frac{B_0}{\omega_0}\frac{d\omega_i}{dP} \quad (1)$$

where B_0 is the bulk modulus, ω_0 is the phonon frequency at ambient pressure, and $d\omega_i/dP$ is the frequency derivative of pressure. The parameters can be obtained experimentally from Raman scattering and X-ray diffraction.

Raman scattering measurements are performed at various pressures to investigate the phonon evolutions. The spectra are collected in a small increment up to 9.4 GPa to get reliable results.

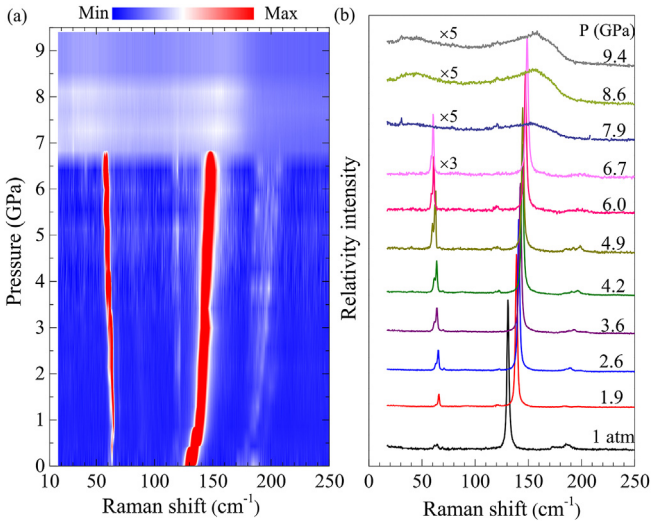

Fig. 3. Raman spectra of $CuInTe_2$ at various pressures. The left color filled contour plot shows the evolution of the phonon frequency shifts and the changes of the full width at the half maximum. The right figure enumerates the raw Raman spectra up to 9.4 GPa.

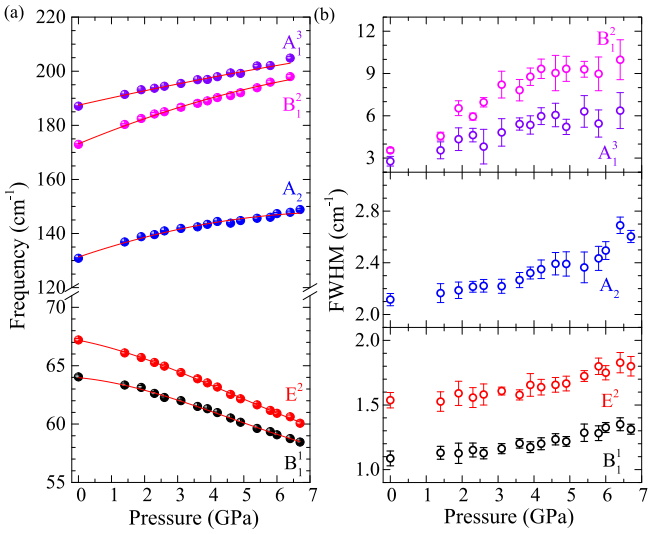

Fig. 4. Lorentz fitted (a) phonon frequencies and (b) FWHMs plotted as functions of pressure. The results are obtained by the Lorentz fitting. The red solid lines in (a) are obtained by the quadratic fitting. (For interpretation of the references to color in this figure legend, the reader is referred to the Web version of this article.)

The phonon evolutions are shown in Fig. 3(a), and the details can be inferred from the raw spectra shown in Fig. 3(b). Five characteristic phonon bands are survived at room temperature. A^1_1, A^2_1, and E^3 modes are vanished due to their sharply reduced intensities around room temperature, suggesting the strong phonon anharmonicity or low vibrational stability of these modes. The low-frequency phonon modes B^1_1 and E^2 clearly show a softening behavior with increasing pressure, and the relative intensities are enhanced. On the contrast, the rest phonon modes exhibit the opposite behaviors. As phonon frequencies are usually hardening in the systems under pressure, the anomalous frequency softening of $CuInTe_2$ imply lattice instability [38] and consequent structural phase transitions [39]. This benefits the enhancement of phonon anharmonicity. The pressure dependent frequencies are fitted by a function of pressure [35]:

$$\omega_i(P) = \omega_i(0) + \frac{d\omega_i}{dP}P + \frac{d^2\omega_i}{dP^2}P^2 \quad (2)$$

where the coefficients reflect the shifting rates of Raman modes. The frequencies follow this equation very well, suggesting the fitted results reliable. The parameters are summarized in the Table 2. The negative coefficients of B^11 and E^2 modes accounts for the lower frequency shifts compared with the high energy modes. Above 6.7 GPa, the phonon intensities are significantly reduced and vanished around 7.9 GPa, consistent with the lattice structure transition.

The FWHMs are directly related to the phonon scattering ratios or lifetimes [40,41] (see Fig. 4). Considering the uncertainty principle, the relation between FWHMs and the phonon lifetime can be described as $\tau_i = 1/2\pi$FWHM. Thus, the FWHMs are applied to investigate the evolution of $CuInTe_2$ phonon lifetimes. The results are obtained by the Lorentz fitting and plotted as functions of pressure in Fig. 5. The FWHMs of higher energy bands are much larger compared with the lower energy bands. The phonon lifetimes of the A_2, B^21, and A^31 bands are much lower, thus occupying lower proportion of the heat conduction. With increasing pressure, all the FWHMs are enhanced, suggesting the reductions of the phonon lifetimes. This result is consistent with the pressure induced κ reduction in our previous work [15]. The high energy bands characterize more significant FWHM broadening compared with the low energy bands. To further reduce the κ of $CuInTe_2$, strategies to enhance the phonon anharmonicity of the low energy bands are crucial.

Next, the pressure dependent X-ray diffraction measurements are performed (Fig. 5) to determine the bulk modulus. Below 7.6 GPa, $CuInTe_2$ keeps the same lattice structure as that at ambient pressure, without new peaks arising or peaks splitting in this range. All the peak angles shift to higher values, suggesting the compression of lattice volume. Above 7.6 GPa, the profiles are changed into a new configuration, and the peak widths are broaden. This is consistent with the Raman spectra, demonstrating the phase transition. In the detected pressure range, no significant hybrid phases are observed. Similar phase transition has been previously observed in this system [42,43].

The XRD patterns can be fitted well with the $I\bar{4}2d$ structure before the phase transition, and a *d-Cmcm* (a distortion of the *Cmcm*) structure after the phase transition. Two typical patterns and the corresponding lattice structures are shown in Fig. 6. The fitting yields reasonable factors of $R_p = 2.6\%$; $R_{wp} = 3.9\%$, and $\chi^2 = 2.9\%$ for 2.3 GPa, and $R_p = 4.4\%$; $R_{wp} = 4.2\%$, and $\chi^2 = 3.7\%$ for 9.1 GPa. The molecule atoms Z are 8 and 4 for $I\bar{4}2d$ and $d-Cmcm$ phase respectively. The lattice parameters a, b, c, and the molecule volume (V/Z) as functions of pressure are obtained from the Rietveld refinement in GSAS [26]. The results are plotted in Fig. 7. In the upper panel, all the lattice parameters are compressed with increasing pressure. The compression ratio along a axis is larger over that of c axis in $I\bar{4}2d$ phase. This illustrates the anisotropic lattice properties, again demonstrating the asymmetric configuration of the chemical bonds. The continuous lines represent fits to a Birch-Murnaghan's equation of state (BM-EOS) expresses as [44]:

$$P = \frac{3}{2}B_0\left(\frac{V}{V_0}\right)^{7/3}\left\{1 + \frac{3}{4}\left(B_0' - 4\right)\left[\left(\frac{V}{V_0}\right)^{3/2} - 1\right]\right\} \quad (3)$$

where V_0 is the unit-cell volume at ambient pressure, and B_0' is the derivative of B_0. As moderate zT has been achieved in the $I\bar{4}2d$ phase, the low pressure patterns are interested in this work.

In the lower panel of Fig. 7, the pressure dependent molecule

Table 2
Summary of the symmetry assignments, the pressure coefficients $d\omega_i/dP$ (cm^{-1}/GPa) and $d^2\omega/dP^2$ (cm^{-1}/GPa^2), and the Grüneisen parameters γ_i for the obtained Raman modes in $CuInTe_2$.

	$B^1{}_1$	E^2	A_2	$B^2{}_1$	$A^3{}_1$
$d\omega_i/dP$ (cm^{-1}/GPa)	−0.75±0.07	−0.90±0.05	4.06±0.26	4.91±0.18	2.68±0.25
$d^2\omega_i/dP^2$ (cm^{-1}/GPa^2)	−0.021±0.01	−0.03±0.01	−0.23±0.04	−0.18±0.03	0.01±0.01
γ_i	−0.77±0.14	−0.82±0.13	1.92±0.32	1.74±0.24	0.89±0.18

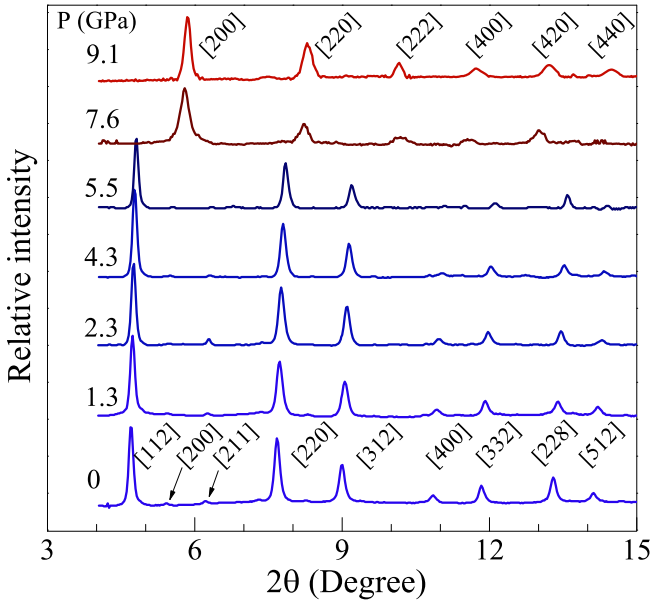

Fig. 5. The evolution of X-ray diffraction patterns collected up to 9.1 GPa.

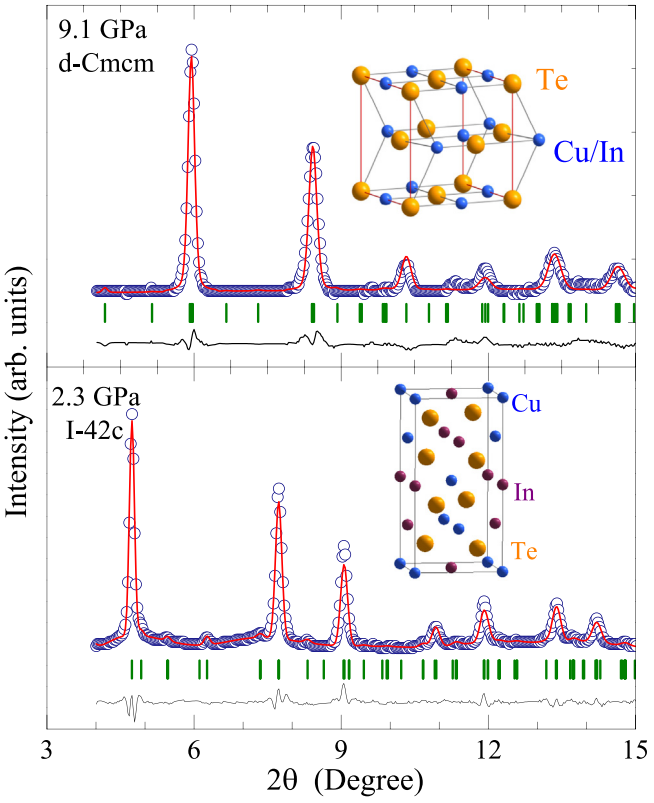

Fig. 6. The selected X-ray diffraction pattern at the pressures of 2.3 and 9.1 GPa. The continuous red line is the fitted result. The difference between the observed and calculated profiles (bottom blue line) is obtained by the Rietveld refinement. The middle sticks refer to the peak positions. The right patterns represent the lattice structures before and after the phase transition. (For interpretation of the references to color in this figure legend, the reader is referred to the Web version of this article.)

volume follows the equation of state very well, thus yielding the reliable B_0=(61.4±5.4) GPa and B_0'=(3.4±0.32) for $I\bar{4}2d$ structure. Compared with other chalcopyrite compounds, the B_0 and phase transition pressure of $CuInTe_2$ are relative low. $CuGaTe_2$, as an example, characterizes B_0 = 76.7 GPa, and the phase transition pressure is higher than $CuInTe_2$ [42]. The bulk modulus thus is able to represent the lattice stability of this system.

Combined the bulk modulus with the phonon frequency shifts, the Grüneisen parameters are determined experimentally. The fitting yields the Grüneisen parameters collected in Table 2. The high frequency phonon modes exhibit relative high γ values compared with the low frequency modes. The A_2, $B^2{}_1$, and $A^3{}_1$ branches are strongly scattered due to the anharmonicity, opposed to those of the low frequency modes. This result is consistent with the evolution of the FWHMs. The negative γ values of $B^1{}_1$ and E^2 modes result from the phonon softening. With increasing pressure, the γ values of $B^1{}_1$, E^2, and $A^3{}_1$ modes are gradually enhanced, while the values of A_2 and $B^2{}_1$ modes are gradually reduced. Pressure enhances the higher order phonon-phonon interaction in $CuInTe_2$, resulting in the enhanced phonon anharmonicity of the low frequency modes.

To estimate the holistic anharmonic effect, the average Grüneisen parameter $\overline{\gamma}$ is represented as the equation: $\overline{\gamma}^2 = \sum \gamma_i^2$. The calculation yields the $\overline{\gamma}$ of the studied vibration modes about 1.22± 0.29. The value is close to the γ of $CuGaTe_2$ (γ∼1) [11], but much lower than those of $AgInTe_2$ (γ = 2.13) and $AgInSe_2$ (γ = 2.27) [45]. The higher anharmonicity in $AgInTe_2$ or $AgInSe_2$ originates from the strong asymmetric configuration of the chemical bonds, in which the Ag-Se(Te) bonding force is much higher over In-Se(Te) bond [45]. While, such effect is weak in $CuInTe_2$ and $CuGaTe_2$ due to the relative low difference between the chemical bonding forces. An evidence is that the optical phonon branches of $AgInSe_2$ or $AgInTe_2$ characterize much lower frequencies. Indeed, $CuInTe_2$ and $CuGaTe_2$ harvest the κ∼7 $Wm^{-1}K^{-1}$ around room temperature [11,15], in comparison with the lower value about 2 $Wm^{-1}K^{-1}$ for $AgInTe_2$ and 1 $Wm^{-1}K^{-1}$ for $AgInSe_2$ [45]. This is intrinsically different with other efficient thermoelectric materials. PbTe and $AgSbTe_2$, as examples, characterize the rock-salt structure with non-bonding *s* and *p* electrons, which is the origin of the high anharmonicity and extremely low κ [46,47]. Intriguingly, $CuInTe_2$ also exhibits a low κ∼1 $Wm^{-1}K^{-1}$ at high temperatures [14], comparable with those of PbTe and $AgSbTe_2$.

Depending on the mode-Grüneisen parameters, the reduction of the heat conduction of the low energy phonon branches is crucial to reduce the κ of $CuInTe_2$. A convenient method is to introduce defects in the lattice. As most of the phonon branches are determined by the vibrations of Cu-Te-In tetrahedrons, the defects on the Cu, In, and Te sites are all effective phonon scattering centers. Nano structure and micrometer composites are also good choices to reduce the long mean free path phonons. Most importantly, it is a

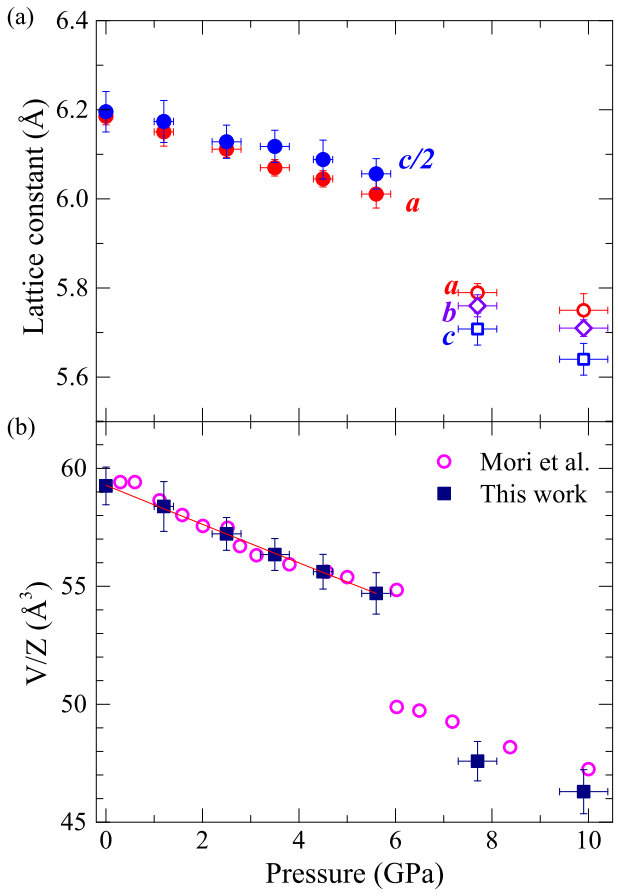

Fig. 7. The lattice parameters and the molecule volume of $CuInTe_2$ plotted as functions of pressure up to 9.1 GPa. The curves are the fitting results of the Birch-Murnaghan's Equation of State.

candidate strategy to reduce thermal conductivity via a high pressure route that induces the phonon softening and lattice instability.

5. Conclusions

We have investigated the phonon dynamic properties of $CuInTe_2$ by a combined computational and experimental study. The phonon dispersion and density of states from *ab initio* calculations revealed the essential contribution of the low energy optic phonon branches. Raman scattering and X-ray diffraction experiments were also performed to detect the phonon and lattice structure evolution under pressure. The optic phonon branches from Raman scattering conformed the phonon dispersion from the *ab initio* calculations. The phase transition around 6 GPa is a result of the lattice instability. This conformed to the relative low bulk modulus. Combined these results, the mode-Grüneisen parameters were firstly determined experimentally. Low energy optic phonon branches characterize small Grüneisen parameters, which are responsible for the high thermal conductivity at modest temperatures. The phonon frequency softening and FWHM broadening were also observed under pressure, suggesting the enhancement of phonon anharmonicity. Our study demonstrates that applying pressure is a feasible strategy for the κ reduction and thermoelectric performance enhancement.

Author contribution statement

Hao Yu: Investigation, Writing-Original Draft, Visualization. Ge Huang: Investigation. Qing Peng: Software. Liu-Cheng Chen: Writing-Review & Editing. Hong-Jie Pang: Writing-Review & Editing. Xiao-Ying Qin: Writing-Review & Editing, Funding acquisition. Peng-Fei Qiu: Resources. Xun Shi: Funding acquisition. Li-Dong Chen: Funding acquisition. Xiao-Jia Chen: Conceptualization, Supervision, Project administration, Writing-Review & Editing.

Declaration of competing interest

The authors declare that they have no known competing financial interests or personal relationships that could have appeared to influence the work reported in this paper.

Acknowledgments

Xun Shi and Li-Dong Chen acknowledged the support from the National Key Research and Development Program of China (No. 2018YFB0703600), the National Natural Science Foundation of China (Grant Nos. 51625205 and 51632010). Xiao-Ying Qin acknowledged the support from the Natural Science Foundation of China under Grant Nos. 51672278, 11674322, and 11374306.

References

[1] M. Zebarjadi, K. Esfarjani, M.S. Dresselhaus, Z.F. Ren, G. Chen, Perspectives on thermoelectrics: from fundamentals to device applications, Energy Environ. Sci. 5 (2012) 5147–5162.
[2] G.J. Snyder, E.S. Toberer, Complex thermoelectric materials, Nat. Mater. 7 (2008) 105–114.
[3] G.J. Snyder, T.S. Ursell, Thermoelectric efficiency and compatibility, Phys. Rev. Lett. 91 (2003) 148301.
[4] H. Alam, S. Ramakrishna, A review on the enhancement of figure of merit from bulk to nano-thermoelectric materials, Nano Energy 7 (2013) 190–212.
[5] Z.F. Ren, Y.C. Lan, Q.Y. Zhang, Advanced Thermoelectrics: Materials, Contacts, Devices, and Systems, CRC Press, 2017.
[6] P. Qiu, X. Shi, L. Chen, Cu-based thermoelectric materials, Energy Storage Materials 3 (2016) 85–97.
[7] X. Shi, L. Chen, C. Uher, Recent advances in high-performance bulk thermoelectric materials, Internal. Mater. Rev. 61 (2016) 379–415.
[8] J. Zhang, R. Liu, N. Cheng, Y. Zhang, J. Yang, C. Uher, X. Shi, L. Chen, W. Zhang, High-performance pseudocubic thermoelectric materials from non-cubic chalcopyrite compounds, Adv. Mater. 26 (2014) 3848–3853.
[9] F.-J. Fan, L. Wu, S.-H. Yu, Energetic I-III-VI_2 and I_2-II-IV-VI_4 nanocrystals: synthesis, photovoltaic and thermoelectric applications, Energy Environ. Sci. 7 (2013) 190–208.
[10] M.G. Panthani, V. Akhavan, B. Goodfellow, J.P. Schmidtke, B.A. Korgel, Synthesis of CuInS2, $CuInSe_2$, and $Cu(InxGa_{1-x})Se_2$ (CIGS) nanocrystal for printable photovoltaics, J. Am. Chem. Soc. 130 (2009) 16770–16777.
[11] T. Plirdpring, K. Kurosaki, A. Kosuga, T. Day, S. Firdosy, V. Ravi, G.J. Snyder, A. Harnwunggmoung, T. Sugahara, Y. Ohishi, Chalcopyrite $CuGaTe_2$: a high-efficiency bulk thermoelectric material, Adv. Mater. 24 (2012) 3622–3626.
[12] B. Wang, H. Xiang, J. Zhou, B. Li, T. Nakayama, Theoretical investigation on thermoelectric properties of Cu-based chalcopyrite compounds, Phys. Rev. B 95 (2017), 035201.
[13] R. Liu, Y. Qin, N. Cheng, J. Zhang, X. Shi, Y. Grin, L. Chen, Thermoelectric performance of $Cu_{1-x-\delta}AgxInTe_2$ diamond-like materials with a pseudocubic crystalstructure, Inorg. Chem. Front. 47 (2016) 1167–1177.
[14] R. Liu, L. Xi, H. Liu, X. Shi, W. Zhang, L. Chen, Ternary compound $CuInTe_2$: a promising thermoelectric material with diamond-like structure, Chem. Commun. 48 (2012) 3818–3820.
[15] H. Yu, L.C. Chen, H.J. Pang, X.Y. Qin, P.F. Qiu, X. Shi, L.D. Chen, X.J. Chen, Large enhancement of thermoelectric performance in $CuInTe_2$ upon compression, Mater. Today Phys. 5 (2018) 1–6.
[16] L.-C. Chen, H. Yu, H.-J. Pang, B.-B. Jiang, L. Su, X. Shi, L.-D. Chen, X.-J. Chen, Pressure-induced enhancement of thermoelectric performance in palladium sulfide, Mater. Today Phys. 5 (2018) 64–71.
[17] L.-C. Chen, P.-Q. Chen, W.-J. Li, Q. Zhang, V.V. Struzhkin, A.F. Goncharov, Z. Ren, X.-J. Chen, Enhancement of thermoelectric performance across the topological phase transition in dense lead selenide, Nat. Mater. 18 (2019) 1321–1326.
[18] N. Cheng, R. Liu, S. Bai, X. Shi, L. Chen, Enhanced thermoelectric performance in Cd doped $CuInTe_2$ compounds, J. Appl. Phys. 115 (2014) 163705.
[19] M.G. Holland, Analysis of lattice thermal conductivity, Phys. Rev. 132 (1963) 2461–2471.
[20] J. Callaway, Model for lattice thermal conductivity at low temperatures, Phys. Rev. 113 (1959) 1046–1051.
[21] Z. Tian, J. Garg, K. Esfarjani, T. Shiga, J. Shiomi, G. Chen, Phonon conduction in

PbSe, PbTe, and $PbTe_{1-x}Se_x$ from first-principles calculations, Phys. Rev. B 85 (2012) 184303.
[22] W. Li, J. Carrete, G.K.H. Madsen, N. Mingo, Influence of the optical-acoustic phonon hybridization on phonon scattering and thermal conductivity, Phys. Rev. B 93 (2016) 205203.
[23] C. Rincón, F.J. Ramirez, Lattice vibrations of CuInSe2 and $CuGaSe_2$ by Raman microspectrometry, J. Appl. Phys. 72 (1992) 4321–4324.
[24] R. Mittal, S.L. Chaplot, H. Schober, T.A. Mary, Origin of negative thermal expansion in cubic ZrW_2O_8 revealed by high pressure inelastic neutron scattering, Phys. Rev. Lett. 86 (2001) 4692–4695.
[25] A.M. Lindenberg, I. Kang, S.L. Johnson, T. Missalla, P.A. Heimann, Z. Chang, J. Larsson, P.H. Bucksbaum, H.C. Kapteyn, H.A. Padmore, R.W. Lee, J.S. Wark, R.W. Falcone, Time-resolved x-ray diffraction from coherent phonons during a laser-induced phase transition, Phys. Rev. Lett. 84 (2000) 111–114.
[26] B.H. Toby, EXPGUI, a graphical user interface for GSAS, J. Appl. Crystallogr. 34 (2001) 210–213.
[27] W. Setyawan, S. Curtarolo, High-throughput electronic band structure calculations: challenges and tools, Comput. Mater. Sci. 49 (2010) 299–312.
[28] S. Clark, M. Segall, C. Pickard, P. Hasnip, M. Probert, K. Refson, M. Payne, First principles methods using CASTEP, Z. Krist. 220 (2005) 5–6.
[29] D. Porezag, M.R. Pederson, Infrared intensities and Raman-scattering activities within density-functional theory, Phys. Rev. B 54 (1996) 7830–7836.
[30] S. Baroni, S. de Gironcoli, A. Dal Corso, P. Giannozzi, Phonons and related crystal properties from density-functional perturbation theory, Rev. Mod. Phys. 73 (2001) 515–562.
[31] A.M. Mintairov, N.A. Sadchikov, T. Sauncy, M. Holtz, G.A. Seryogin, S.A. Nikishin, H. Temkin, Vibrational Raman and infrared studies of ordering in epitaxial $ZnSnP_2$, Phys. Rev. B 59 (1999) 15197–15207.
[32] J. Yang, S. Chen, Z. Du, X. Liu, J. Cui, Lattice defects and thermoelectric properties: the case of p-type $CuInTe_2$ chalcopyrite on introduction of zinc, Dalton Trans. 43 (2014) 15228–15236.
[33] Y. Li, Q. Meng, Y. Deng, H. Zhou, Y. Gao, Y. Li, J. Yang, J. Cui, High thermoelectric performance of solid solutions $CuGa_{1-x}InxTe_2$ (x= 0-1.0), Appl. Phys. Lett. 100 (2012) 231903.
[34] E.F. Lambson, W.A. Lambson, J.E. Macdonald, M.R.J. Gibbs, G.A. Saunders, D. Turnbull, Elastic behavior and vibrational anharmonicity of a bulk $Pd_{40}Ni_{40}P_{20}$ metallic glass, Phys. Rev. B 33 (1986), 053122.
[35] G. Lucazeau, Effect of pressure and temperature on Raman spectra of solids: anharmonicity, J. Raman Spectrosc. 34 (2003) 478–496.
[36] L.-C. Chen, Q. Peng, H. Yu, H.-J. Pang, B.-B. Jiang, L. Su, X. Shi, L.-D. Chen, X.-J. Chen, Lattice dynamics of thermoelectric palladium sulfide, J. Alloy. Comp. 798 (2019) 484–492.
[37] H.-J. Pang, L.-C. Chen, Z.-Y. Cao, H. Yu, C.-G. Fu, T.-J. Zhu, A. Goncharov, X.-J. Chen, Mode Grüneisen parameters of an efficient thermoelectric half-heusler, J. Appl. Phys. 124 (2018) 195107.
[38] C. Carlone, D. Olego, A. Jayaraman, M. Cardona, Pressure dependence of the Raman modes and pressure-induced phase changes in $CuGaS_2$, and $AgGaS_2$, Phys. Rev. B 22 (1980) 3877–3885.
[39] A.K. Arora, Grüneisen parameter of soft phonons and high pressure phase transitions in semiconductors, J. Phys. Chem. Solids 51 (1990) 373–375.
[40] L. Bergman, D. Alexson, P.L. Murphy, R.J. Nemanich, M. Dutta, M.A. Stroscio, C. Balkas, H. Shin, R.F. Davis, Raman analysis of phonon lifetimes in AlN and GaN of wurtzite structure, Phys. Rev. B 59 (1999) 12977–12982.
[41] R. Cuscó, E. Alarcón-Lladó, J. Ibáñez, L. Artús, J. Jiménez, B. Wang, M.J. Callahan, Temperature dependence of Raman scattering in ZnO, Phys. Rev. B 75 (2007) 165202.
[42] Y. Mori, T. Ikai, K. Takarabe, High-pressure phase in the chalcopyrites $CuGaTe_2$ and $CuInTe_2$, Phys. Status Solidi 2 (2003) 317–320.
[43] T. Bovornratanaraks, V. Saengsuwan, K. Yoodee, M.I. McMahon, C. Hejny, D. Ruffolo, High pressure orthorhombic structure of $CuInSe_2$, J. Phys. Condens. Matter 22 (2010) 355801.
[44] F. Birch, Finite elastic strain of cubic crystals, Phys. Rev. 71 (1947) 809–824.
[45] P. Qiu, Y. Qin, Q. Zhang, R. Li, J. Yang, Q. Song, Y. Tang, S. Bai, X. Shi, L. Chen, Intrinsically high thermoelectric performance in $AgInSe_2$ n-type diamond-like compounds, Adv. Sci. 5 (2018) 1700727.
[46] D.T. Morelli, V. Jovovic, J.P. Heremans, Intrinsically minimal thermal conductivity in cubic I-V-VI_2 semiconductors, Phys. Rev. Lett. 101 (2008), 035901.
[47] J.P. Heremans, The anharmonicity blacksmith, Nat. Phys. 11 (2015) 990–991.